Alexandria Engineering Journal (2016) 55, 2157–2169

Alexandria University

Alexandria Engineering Journal

www.elsevier.com/locate/aej
www.sciencedirect.com

ORIGINAL ARTICLE

Magneto-hydrodynamic natural convection in an inclined T-shaped enclosure for different nanofluids and subjected to a uniform heat source

Ahmed Kadhim Hussein [a,*], **M.A.Y. Bakier** [b], **Mohamed Bechir Ben Hamida** [c,d], **S. Sivasankaran** [e]

[a] *College of Engineering, Mechanical Engineering Department, Babylon University, Babylon City, Hilla, Iraq*
[b] *Department of Mathematics, Faculty of Sciences, Assiut University, Assiut, Egypt*
[c] *High School of Sciences and Technology of Hammam Sousse (ESSTHS), Department of Physics, University of Sousse, Sousse, Tunisia*
[d] *Research Unit of Ionized Backgrounds and Reagents Studies (UEMIR), Preparatory Institute for Engineering Studies of Monastir (IPEIM), University of Monastir, Monastir City, Tunisia*
[e] *Institute of Mathematical Sciences, University of Malaya, Kuala Lumpur 50603, Malaysia*

Received 17 February 2016; revised 13 June 2016; accepted 25 June 2016
Available online 19 July 2016

KEYWORDS

Nanofluid;
Natural convection;
Magnetic field;
T-shaped enclosure;
Heat source

Abstract This paper examines numerically by using the finite difference method the laminar steady magneto-hydrodynamic natural convection in an inclined T-shaped enclosure filled with different types of nanofluids. A uniform heat source is embedded on a part of the upper wall of the enclosure. Both left and right sidewalls of the enclosure leg are maintained at a constant cold temperature, while the other portions of the enclosure walls are considered adiabatic. A magnetic field is applied vertically downward on the bottom wall of the enclosure. Based on the numerical results, the effects of the dominant parameters such as Rayleigh number, Hartmann number, inclination angle, solid volume fraction, location and length of the heat source and enclosure aspect ratio are examined. The numerical results are obtained for Hartmann number varying as $0 \leqslant Ha \leqslant 100$, inclination angle varying as $0 \leqslant \Phi \leqslant 90°$, Rayleigh numbers varying as $10^3 \leqslant Ra \leqslant 10^6$, aspect ratio $0.3 \leqslant \mathrm{AR} \leqslant 0.9$, heat source length $0.2 \leqslant B \leqslant 0.8$, heat source location $0.2 \leqslant D \leqslant 0.5$ and the solid volume fractions varying as $0 \leqslant \phi \leqslant 0.2$. Comparison with previously published numerical work is performed and a good agreement between the results is observed. It is found that the mean Nusselt number increases with the increase of Rayleigh number, inclination angle, aspect ratio, heat source location and volume fraction of nanoparticles, while, it decreases when the Hartmann number and heat source length increase.

* Corresponding author.
E-mail address: ahmedkadhim7474@gmail.com (A.K. Hussein).

Peer review under responsibility of Faculty of Engineering, Alexandria University.

http://dx.doi.org/10.1016/j.aej.2016.06.020

Nomenclature

AR	aspect ratio
B_o	magnitude of the magnetic field (T)
B	dimensionless heat source length
bb	dimensional heat source length (m)
c_p	specific heat at constant pressure (J/kg °C)
D	dimensionless heat source location
dd	dimensional heat source location (m)
g	gravitational acceleration (m/s^2)
H	width of enclosure head (m)
h	convection heat transfer coefficient (W/m^2 °C)
Ha	Hartmann number
k	thermal conductivity (W/m °C)
Nu	Nusselt number
P	dimensionless Pressure
p	pressure (N/m^2)
Pr	Prandtl number
Ra	Rayleigh number
T	temperature (°C)
U	dimensionless velocity component in X-direction
u	velocity component in x-direction (m/s)
V	dimensionless velocity component in Y-direction
v	velocity component in y-direction (m/s)
W	width of enclosure leg
X	dimensionless coordinate in horizontal direction
x	Cartesian coordinate in horizontal direction (m)
Y	dimensionless coordinate in Y-direction
y	Cartesian coordinate in vertical direction (m)

Greek symbols

α	thermal diffusivity (m^2/s)
Ω	dimensionless vorticity
ψ	dimensionless stream function
Ψ	stream function (m^2/s)
β	coefficient of thermal expansion (K^{-1})
θ	dimensionless temperature
σ	electrical conductivity (W/m °C)
ϕ	solid volume fraction
ν	kinematic viscosity of the fluid (m^2/s)
μ	viscosity of the fluid (kg/m s)
ρ	density (kg/m^3)
ψ	dimensionless stream function
Φ	enclosure inclination angle

Subscripts

c	cold
f	fluid particle
h	hot
Loc	local
nf	nano fluid property
m	mean or average
p	solid particle

1. Introduction

Nanofluids are dilute liquid suspensions of nanoparticles with at least one critical dimension smaller than 100 nm. Nowadays, more attention is considered to this new type of composite material because of its enhanced properties and behavior associated with the heat transfer. The main problems of using such suspensions are the rapid settling of particles, clogging of flow channels, and increased pressure drop in the fluid [1,2]. From the other side, the term magneto-hydrodynamics (MHD) or sometimes called 'magneto-convection' summarizes the variety of processes arising from the dynamic interaction between convective motions and magnetic fields in an electrically conducting medium. MHD natural convection flows are encountered in numerous problems covering a wide range of basic sciences such as astrophysics, fire research, metallurgy and nuclear engineering [3]. Natural convection inside irregular geometries has a wide application in engineering and industry. Investigations on the pure and MHD natural convection in irregular cavities filled with nanofluid have been done by many researchers. Mahmoodi [4] investigated numerically the free convection of Cu-water nanofluid inside L-shaped cavities by using the finite volume method. The results indicated that for all Rayleigh numbers considered, the average Nusselt number increased when the aspect ratio of the cavity and the solid volume fraction increased. Mahmoodi and Hashemi [5] studied numerically the natural convection of Cu-water nanofluid inside C-shaped enclosure. They concluded that as the C-shaped enclosure became narrower, the rate of heat transfer increased. Also, as the Rayleigh number increased, the rate of heat transfer increased for a constant aspect ratio. Dehnavi and Rezvani [6] performed a numerical investigation on the natural convection of water-Al_2O_3 nanofluid in a Γ shaped cavity. Results indicated that using nanofluid caused an increase in the Nusselt number. Mansour et al. [7] studied numerically the natural convection of Cu-water nanofluid inside T-shaped enclosure. It was found that as the T-shaped enclosure became narrower, the rate of heat transfer increased. Ali et al. [8] investigated experimentally the natural convection inside a vertical circular enclosure heated from below and filled with water-based Al_2O_3 nanofluids. Four various concentrations (0.0, 0.21, 0.51 and 0.75 percentage by volume) were used. General correlations were obtained for the average Nusselt numbers versus the modified Rayleigh numbers using the volume concentration ratio as a parameter for each enclosure. Kalteh and Hasani [9] used the lattice Boltzmann method to investigate the free convection in L-shaped enclosure filled with alumina/water nanofluid. It was found that the rate of the heat transfer enhancement with volume concentration was higher for lower aspect ratios. Very recently, Rahman et al. [10] performed a numerical simulation of unsteady natural convection in a half-moon shape enclosure with variable thermal boundary condition and different nanofluids. It was found that for higher values of solid volume fraction and Rayleigh number, the heat transfer characteristics improved. Further references can be found in [11–21]. Sourtiji and Hosseinizadeh [22] studied numerically the flow and heat transfer characteristics of alumina-water nanofluid on natural convection inside L-shaped cavities in the presence of an external magnetic field. The results showed that the heat transfer

was augmented by adding the nanoparticles to the base fluid and increased with solid volume fraction of the nanofluid. Sheikholeslami et al. [23] investigated the effect of a magnetic field on natural convection in an inclined half-annulus enclosure filled with Cu–water nanofluid using CVFEM. The effects of Hartmann number, Rayleigh number, volume fraction of nanoparticle and inclination angle on the flow and heat transfer characteristics were investigated. The results indicated that the magnetic field damped the flow and the temperature oscillations by reducing the fluid velocity and Nusselt number. Sheikholeslami et al. [24] investigated numerically by using LBM, the magneto-hydrodynamics free convection in a semi-annulus enclosure filled with Al_2O_3-water nanofluid. They found that the enhancement in the heat transfer increased as the Hartmann number increased but it decreased with the increase of the Rayleigh number. Al-Zamily [25] investigated numerically using the finite element methods the effect of magnetic field on the natural convection in a semicircular shape cavity filled with Cu–water nanofluid and heated by heat flux source at the base wall. He concluded that the strength of convection effect increased as the Rayleigh number increased and diminished as the Hartmann number increased. Sheikholeslami et al. [26] studied numerically the MHD effect on natural convection in an inclined L-shape enclosure filled with nanofluid. They concluded that the inclination angle of the enclosure could be considered as a control parameter for heat and fluid flow. Also, the Nusselt number was an increasing function of Rayleigh number and volume fraction of nanoparticles and a decreasing function of Hartmann number and inclination angle. Very recently, Sheikholeslami et al. [27] investigated numerically the MHD free convection of Al_2O_3-water nanofluid in the semi-annulus enclosure. The results showed that the Nusselt number had a direct relationship with buoyancy ratio number, while it had a reverse relationship with both Hartmann and Lewis numbers. Based on the above literature review and due to the lack of information about T-shaped enclosure, the present work investigates for the first time the magneto-hydrodynamic natural convection in an inclined T-shaped enclosure filled with different types of nanofluids.

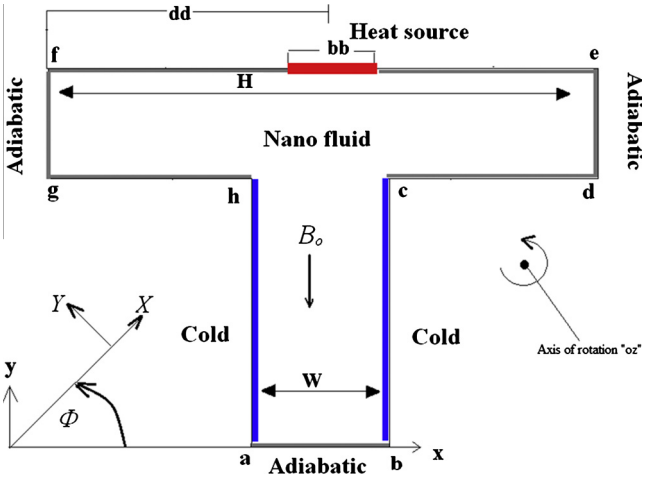

Figure 1 Physical model of the problem.

2. Problem formulation

Fig. 1 depicts the schematic view and coordinates of a two-dimensional inclined T-shaped enclosure. An uniform heat source is embedded on a part of the upper wall of the enclosure. Both left and right sidewalls of the enclosure leg are maintained at a cold temperature (T_c). The adiabatic portions of the enclosure walls are shown in Fig. 1. The fluid inside the enclosure is a water based nanofluid containing different types of solid spherical nanoparticles which are Cu, Ag, Al_2O_3, and TiO_2. A magnetic field of magnitude (B_o) is applied vertically downward on the enclosure. The gravitational force is assumed to act in the negative y-direction. The thermo-physical properties of the base fluid and nanoparticles are given in Table 1. The governing equations are simplified by using the following assumptions:

1. The thermo-physical properties of both the base fluid and nanofluid are assumed to be constant except for the density variation, which is modeled using Boussinesq model.
2. The nanoparticles have a uniform size and shape and are well dispersed within the base fluid.
3. It is assumed that the base fluid (i.e. water) and nanoparticles are in thermal equilibrium state and no slip occurs between liquid and nanofluid phases in terms of both velocity and temperature.
4. The flow field is considered two dimensional, Newtonian, laminar and steady.
5. The effects of the radiation and the wall cavity thickness are assumed negligible.

3. Governing equations

The dimensionless governing equations for the laminar and steady state magneto-hydrodynamic natural convection in a two-dimensional inclined T-shaped enclosure are given by

$$\frac{\partial U}{\partial X}+\frac{\partial V}{\partial Y}=0, \tag{1}$$

Table 1 Thermo-physical properties of water and nanoparticles.

Property	Pure water	Copper (Cu)	Silver (Ag)	Alumina Al_2O_3	Titanium oxide (TiO_2)
ρ (kg m^{-3})	997.1	8933	10,500	3970	4250
C_p (J kg^{-1} K^{-1})	4179	385	235	765	686.2
k (W m^{-1} K^{-1})	0.613	401	429	40	8.9538
β (K^{-1})	21×10^{-5}	1.67×10^{-5}	1.89×10^{-5}	0.85×10^{-5}	0.9×10^{-5}
σ ((Ω m)$^{-1}$)	0.05	5.96×10^{7}	–	–	–

$$\Omega = \frac{\partial V}{\partial X} - \frac{\partial U}{\partial Y} = -\nabla^2 \psi, \tag{2}$$

$$U\frac{\partial \Omega}{\partial X} + V\frac{\partial \Omega}{\partial Y} = \frac{\mu_{nf}}{\rho_{nf}\alpha_f}\left(\frac{\partial^2 \Omega}{\partial X^2} + \frac{\partial^2 \Omega}{\partial Y^2}\right) + Ha^2\ Pr\frac{\sigma_{nf}}{\sigma_f}\frac{\rho_f}{\rho_{nf}}\left[\cos^2\Phi\frac{\partial U}{\partial Y} + 2\cos\Phi\sin\Phi\frac{\partial U}{\partial X} - \sin^2\Phi\frac{\partial V}{\partial X}\right] + Ra\ Pr\frac{\rho_f}{\rho_{nf}}\left[1 - \varphi + \frac{(\rho\beta)_{nf}}{(\rho\beta)_f}\varphi\right]\left(\cos\Phi\frac{\partial \theta}{\partial Y} - \sin\Phi\frac{\partial \theta}{\partial X}\right), \tag{3}$$

$$U\frac{\partial \theta}{\partial X} + V\frac{\partial \theta}{\partial Y} = \frac{\alpha_{nf}}{\alpha_f}\left(\frac{\partial^2 \theta}{\partial X^2} + \frac{\partial^2 \theta}{\partial Y^2}\right), \tag{4}$$

These dimensionless governing equations have been obtained by employing the following non-dimensional variables as listed below:

$$X = \frac{x}{H} \quad Y = \frac{y}{W} \quad U = \frac{uH}{\alpha_f} \quad V = \frac{vH}{\alpha_f} \quad P = \frac{pH^2}{\rho_f \alpha_f^2}$$
$$\mathrm{AR} = \frac{H}{W} \quad B = \frac{bb}{H} \quad D = \frac{dd}{H} \quad \theta = \frac{T - T_c}{T_h - T_c}$$
$$Pr = \left(\frac{v}{\alpha}\right)_f \quad Ra = \frac{g\beta_f[T_h - T_c]H^3}{(v\alpha)_f} \quad Ha = B_o H\sqrt{\frac{\sigma_f}{\rho_f v_f}}, \tag{5}$$

In the above equations, the nanofluid thermal diffusivity, effective density, heat capacitance, coefficient of thermal expansion and the effective viscosity are respectively, given by [28]

$$\alpha_{nf} = \frac{k_{nf}}{(\rho c_p)_{nf}}, \tag{6}$$

$$\rho_{nf} = (1-\phi)\rho_f + \phi\rho_p, \tag{7}$$

$$(\rho c_p)_{nf} = (1-\phi)(\rho c_p)_f + \phi(\rho c_p)_p, \tag{8}$$

$$(\rho\beta)_{nf} = (1-\phi)(\rho\beta)_f + \phi(\rho\beta)_p, \tag{9}$$

$$\mu_{nf} = \frac{\mu_f}{(1-\phi)^{2.5}} \tag{10}$$

while, the effective thermal conductivity of the nanofluid is introduced as [29]

$$\frac{k_{nf}}{k_f} = \frac{(k_p + 2k_f) - 2\phi(k_f - k_p)}{(k_p + 2k_f) + \phi(k_f - k_p)}. \tag{11}$$

The fluid motion inside the T-shaped enclosure is represented by using the dimensionless stream function (ψ) obtained from dimensionless velocity components (U) and (V). The relationships between stream function and velocity components are given by

$$U = \frac{\partial \psi}{\partial Y} \text{ and } V = -\frac{\partial \psi}{\partial X}, \tag{12}$$

where $\psi = \frac{\Psi}{\alpha_f}$.

3.1. Local and average Nusselt number

The local and average Nusselt number can be written as

$$Nu_{\mathrm{Loc}} = \frac{hH}{k_f}, \tag{13}$$

$$Nu_l = \frac{1}{\theta(X)} \text{ on wall (f–e).} \tag{14}$$

$$Nu_m = \int_{D-0.5*B}^{D+0.5*B} Nu_l dX. \tag{15}$$

3.2. Boundary conditions

To simulate the flow and thermal fields in an inclined T-shaped enclosure, the following non-dimensional boundary conditions are considered:

1. Walls (a–b, c–d, g–h) are considered adiabatic, i.e.,

$$\frac{\partial \theta}{\partial Y} = 0, \quad U = 0 \text{ and } V = 0. \tag{16}$$

2. Walls (d–e, f–g) are considered adiabatic, i.e.,

$$\frac{\partial \theta}{\partial X} = 0, \quad U = 0 \text{ and } V = 0, \tag{17}$$

3. Walls (a–h, b–c) are maintained at a constant cold temperature, i.e.,

$$\theta = 0, \quad U = 0 \text{ and } V = 0. \tag{18}$$

4. Heat source region at wall (f–e) is maintained at a constant hot temperature, i.e.,

$$\frac{\partial \theta}{\partial Y} = -\frac{k_{nf}}{k_f}, \quad U = 0, \quad V = 0 \text{ and } D - 0.5*B \leqslant X \leqslant D + 0.5*B. \tag{19}$$

5. Other regions of walls (f–e) are considered adiabatic, i.e.,

$$\frac{\partial \theta}{\partial Y} = 0, \quad U = 0 \text{ and } V = 0. \tag{20}$$

4. Numerical procedure and validation

In this investigation, the finite difference method as described by Mansour et al. [30] is employed to solve the governing equations with the boundary conditions. Central difference quotients are used to approximate the second derivatives in both the X and Y directions. Then, the obtained discretized equations are solved using a Gauss-Seidel iteration technique [31,32]. The solution procedure is iterated until the following convergence criterion is satisfied:

$$\sum_{i,j}\left|\chi_{i,j}^{new} - \chi_{i,j}^{old}\right| \leqslant 10^{-7}, \tag{20}$$

where χ is the general dependent variable. The numerical method is implemented in a FORTRAN program. The finite difference method uses four sets of grids: (36×36, 66×66, 96×96 and 126×126) as shown in Table 2. A good agreement is found between 66×66 and 126×126 grids, so the numerical computations were carried out for 66×66 and 126×126 grid nodal points. In order to verify the accuracy of the present method, the obtained results under special cases are compared with the results obtained by Mansour et al. [7]. Table 3 shows an acceptable agreement between the present

Table 2 Grid independent test at $Ra = 10^5$, $Ha = 50$, $B = 0.3$, $D = 0.5$, $\phi = 0.1$, $\Phi = 0$ and AR = 0.5 for Cu-water nanofluid.

Grid	Nu_m	θ_{max}	$\lvert\psi\rvert_{max}$
36 × 36	4.994	0.208	0.232
66 × 66	5.555	0.189	0.304
96 × 96	5.831	0.181	0.314
126 × 126	6.251	0.169	0.366

Table 3 Validation of the numerical code.

Ra	Nanotypes	Nu_m		θ_{max}	
		Mansour et al. [7]	Present work	Mansour et al. [7]	Present work
10^3	Cu	5.639	4.262	0.194	0.248
	Ag	5.640	4.588	0.194	0.231
	Al_2O_3	5.572	4.903	0.196	0.216
	TiO_2	5.3633	5.099	0.204	0.208
10^4	Cu	5.6179	4.261	0.194	0.248
	Ag	5.6211	4.588	0.194	0.23
	Al_2O_3	5.5359	4.902	0.195	0.215
	TiO_2	5.3272	5.098	0.202	0.207
10^5	Cu	5.6599	4.263	0.187	0.245
	Ag	5.6385	4.588	0.188	0.228
	Al_2O_3	5.8706	4.905	0.177	0.213
	TiO_2	5.7126	5.102	0.181	0.204
10^6	Cu	5.5310	4.292	0.157	0.2403
	Ag	5.4705	4.614	0.158	0.224
	Al_2O_3	5.8025	4.944	0.150	0.209
	TiO_2	5.5903	5.146	0.155	0.2

results and the results obtained by Mansour et al. [7]. This favorable comparison gives a confidence in the numerical results to be reported subsequently.

5. Results and discussion

The magneto-hydrodynamic natural convection flow and heat transfer in an inclined T-shaped enclosure filled with different types of nanofluids has been investigated numerically in this paper. In the present work, the Hartmann number is varied as $0 \leqslant Ha \leqslant 100$, the Rayleigh number is taken as $10^3 \leqslant Ra \leqslant 10^6$, heat source location is varied as $0.2 \leqslant D \leqslant 0.5$ and the heat source length is varied as $0.2 \leqslant B \leqslant 0.8$. The solid volume fractions (ϕ) have been varied as $0 \leqslant \phi \leqslant 0.2$, inclination angle varied as $0 \leqslant \Phi \leqslant 90°$ and aspect ratio varied as $0.3 \leqslant AR \leqslant 0.9$.

5.1. Effect of aspect ratio

Fig. 2 shows streamlines (up) and isotherms (bottom) for various aspect ratios inside the T-shaped enclosure filled with nano fluid ($\phi = 0.1$) at $Ha = 50$, $Ra = 10^5$, $B = 0.3$, $D = 0.5$ and $\Phi = 0$. It can be noticed from this figure that as the aspect ratio increases from [AR = 0.3] to [AR = 0.9], the intensity of the flow circulation increases. Therefore, the values of the stream function increase significantly from low values when the aspect ratio is low [i.e., AR = 0.3], to the high values when the aspect ratio is high [i.e., AR = 0.9]. So, it can be concluded that when the aspect ratio of the enclosure increases, a clear improvement in the flow circulation occurs. Also, it can be noticed from the results that the maximum and minimum limits for the rotating vortices occur in the space between the heat source and the cold sidewalls of the enclosure leg. Furthermore, the size of the rotating vortices increases as the aspect ratio increases. Moreover as the T-shaped enclosure becomes more narrow [i.e., AR = 0.3], the natural convection effect in the region between the enclosure leg and the bottom wall decreases significantly which causes the flow vortices not to be constructed in this region as shown in Fig. 2. With respect to isotherms, it can be shown that when the aspect ratio is low [i.e., AR = 0.3], they are in general smooth and approximately parallel to the upper walls and the heat transfer is purely occurred due to the conduction. But, as the aspect ratio increases, the isotherms begin to extend deeply inside the enclosure leg especially at AR = 0.9. For this case, the isotherms are non-linear which indicates high temperature gradients and the heat is transferred due to convection. For AR = 0.5 a transition from conduction to convection occurs and the vortices are formed in the horizontal part of the enclosure.

5.2. Effect of Rayleigh number

Fig. 3 illustrates streamlines (top) and isotherms (down) inside the T-shape enclosure filled with nano fluid ($\phi = 0.1$) at $Ha = 50$, AR = 0.5, $B = 0.3$, $D = 0.5$ and $\Phi = 0$ for various Rayleigh number. The flow pattern can be characterized by two symmetrical re-circulating vortices adjacent to the cold left and right sidewalls of the enclosure leg. The flow field is created adjacent to the heat source at the top of the enclosure and then cooled by the cold sidewalls of the enclosure leg and compressed as it moves downward. This recycle motion leads to produce the re-circulating vortices inside the enclosure. For low Rayleigh number [$Ra = 10^3$ and 10^4], the viscous force is more dominant than the buoyancy force. In this case, the intensity of circulation is weak and the re-circulating vortices inside the enclosure are symmetrical to each other due to the weak effect of buoyancy force. Therefore, the nature of streamlines and flow field does not change significantly when the Rayleigh number is low. In this case, the natural convection contribution in the heat transfer process is weak. But in the case, when the Rayleigh number is high [$Ra = 10^5$ and 10^6], a strong intensity of circulation can be seen inside the T-shape enclosure. The flow circulation is high in the enclosure center. Also, the center of re-circulating vortices moves downward when the Rayleigh number is high [$Ra = 10^6$]. Moreover, the re-circulating vortices become more irregular in comparison with the corresponding vortices when the Rayleigh number is low. In this case, the buoyancy forces are more dominant than viscous forces and the natural convection contribution in the heat transfer process is high. With respect to the thermal field, for low Rayleigh number [$Ra = 10^3$ and 10^4], isotherms are approximately symmetrical

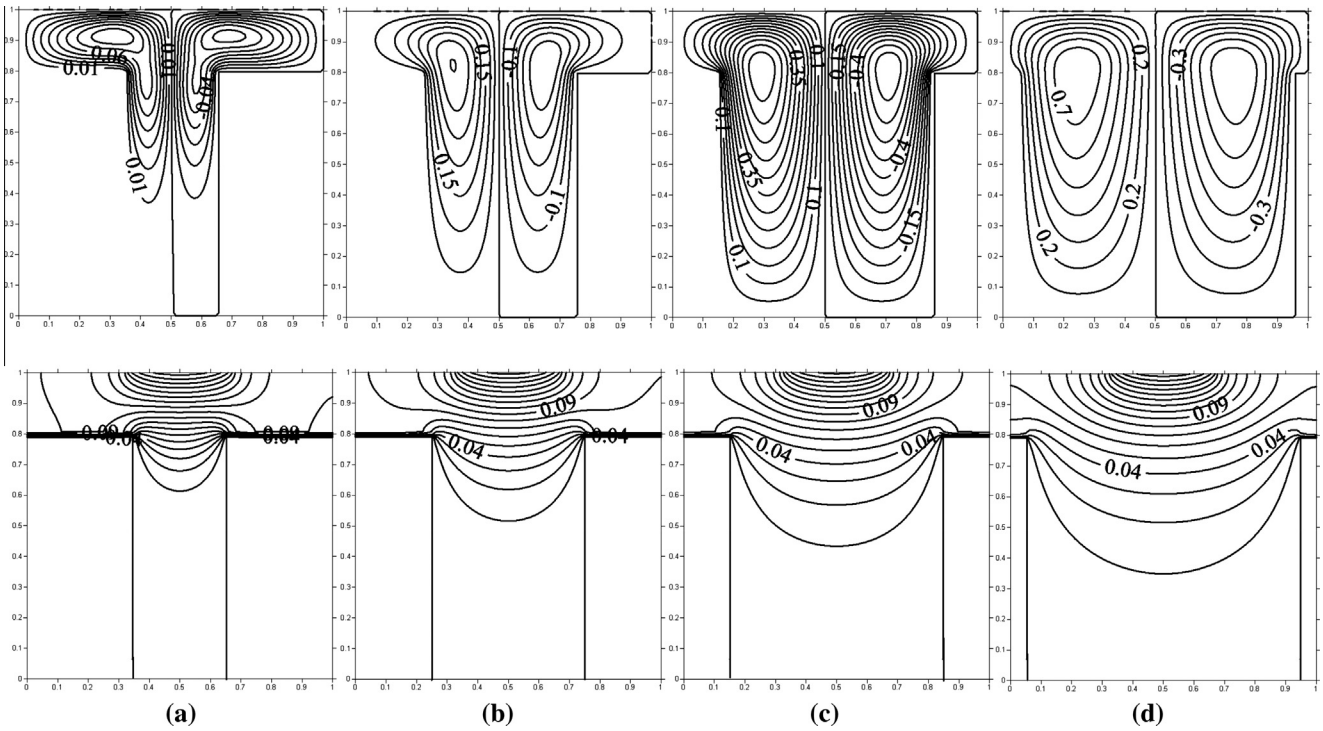

Figure 2 Streamlines (top) and isotherms (down) inside the T-shape enclosure filled with nanofluid ($\phi = 0.1$) at $Ha = 50$, $Ra = 10^5$, $B = 0.3$, $D = 0.5$ and $\Phi = 0$ for various aspect ratio [(a) AR = 0.3, (b) AR = 0.5, (c) AR = 0.7, (d) AR = 0.9].

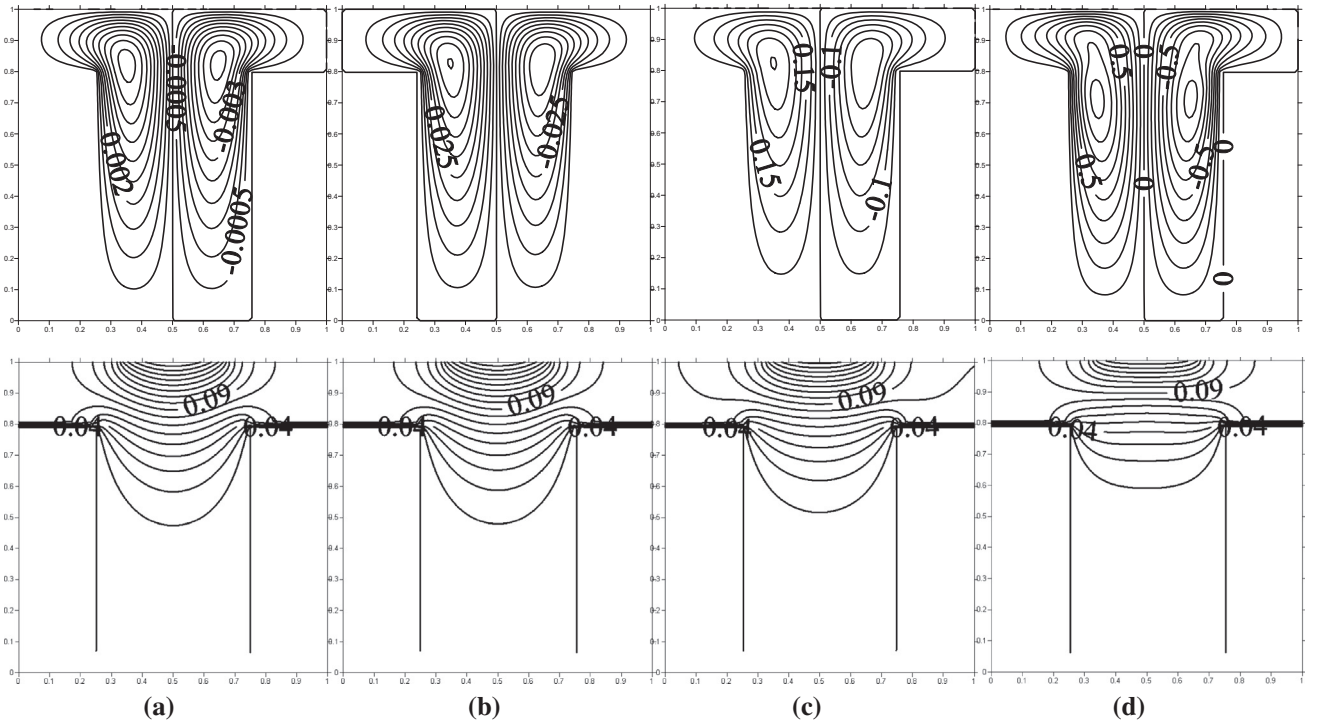

Figure 3 Streamlines (top) and isotherms (down) inside the T-shape enclosure filled with nano fluid ($\phi = 0.1$) at $Ha = 50$, AR = 0.5, $B = 0.3$, $D = 0.5$ and $\Phi = 0$ for various Rayleigh number [(a) $Ra = 10^3$, (b) $Ra = 10^4$, (c) $Ra = 10^5$, (d) $Ra = 10^6$].

and parallel to the upper walls, which indicate that most of the heat is transferred inside the enclosure by the pure conduction. But in the case, when the Rayleigh number is high [$Ra = 10^5$ and 10^6], isotherms are strongly accumulated strongly near the heat source. Furthermore, isotherms change their shape from symmetrical shape to the curved one indicating that most

of the heat is transferred inside the enclosure by convection. Also, it can be noticed from the results that the isotherms are clustered adjacent to the top of the enclosure. This is a logical behavior since the top wall has a maximum effect on the fluid heating due to the existence of the heat source.

5.3. Effect of Hartmann number

Fig. 4 illustrates the streamlines (top) and isotherms (down) inside the T-shape enclosure filled with nanofluid ($\phi = 0.1$) at AR = 0.5, $Ra = 10^5$, $B = 0.3$, $D = 0.5$ and $\Phi = 0$ for various Hartmann number. The Hartmann number represents a measure of the relative importance of the magneto-hydrodynamic flow. When the Hartmann number is zero [$Ha = 0$] or in the other words when the magnetic field is absent, the intensity of circulation is strong, since the buoyancy force due to the natural convection is high. Therefore, the convection heat transfer plays the primary role when the magnetic field effect is negligible which leads to increase the stream function values. But, when the Hartmann number increases [i.e., $Ha = 50$ and 100], the Lorentz force which is created due to the magnetic field effect becomes higher than the buoyancy force which causes to drop the flow circulation intensity and as a result the convection effect begins to decrease significantly. Therefore, it can be observed from Fig. 4, that the stream function values begin to decrease significantly as the Hartmann number increases from [$Ha = 0$] to [$Ha = 100$]. With respect to the thermal field, when the Hartmann number is absent [$Ha = 0$], the isotherms are concentrated highly adjacent to the heat source location and their shape is in general curved which indicates that the heat inside the enclosure is transferred due to the natural convection. When the magnetic field effect is significant or when the Hartmann number increases [$Ha = 50$ and 100], the concentrated region of isotherms adjacent to the heat source location becomes less compressed and isothermal lines become more smooth. This is due to the increase of magnetic field and in this case the heat is transferred inside the enclosure by the pure conduction.

5.4. Effect of solid volume fraction

Fig. 5 explains streamlines (top) and isotherms (down) inside the T-shape enclosure filled with pure and nanofluids at AR = 0.5, $Ra = 10^5$, $B = 0.3$, $D = 0.5$, $Ha = 50$ and $\Phi = 0$ for various solid volume fraction. It can be observed from Fig. 5 that, when the solid volume fraction of nanoparticles increases from [$\phi = 0$] (i.e., pure fluid) to [$\phi = 0.1$], the circulation intensity increases as a result of the high energy transport through the flow related with the high motion of nanoparticles. But as the solid volume fraction increases further to [$\phi = 0.2$], the steam function values begin to decrease strongly. The reason of this behavior is because the high quantities of nanoparticles volume fraction cause a significant

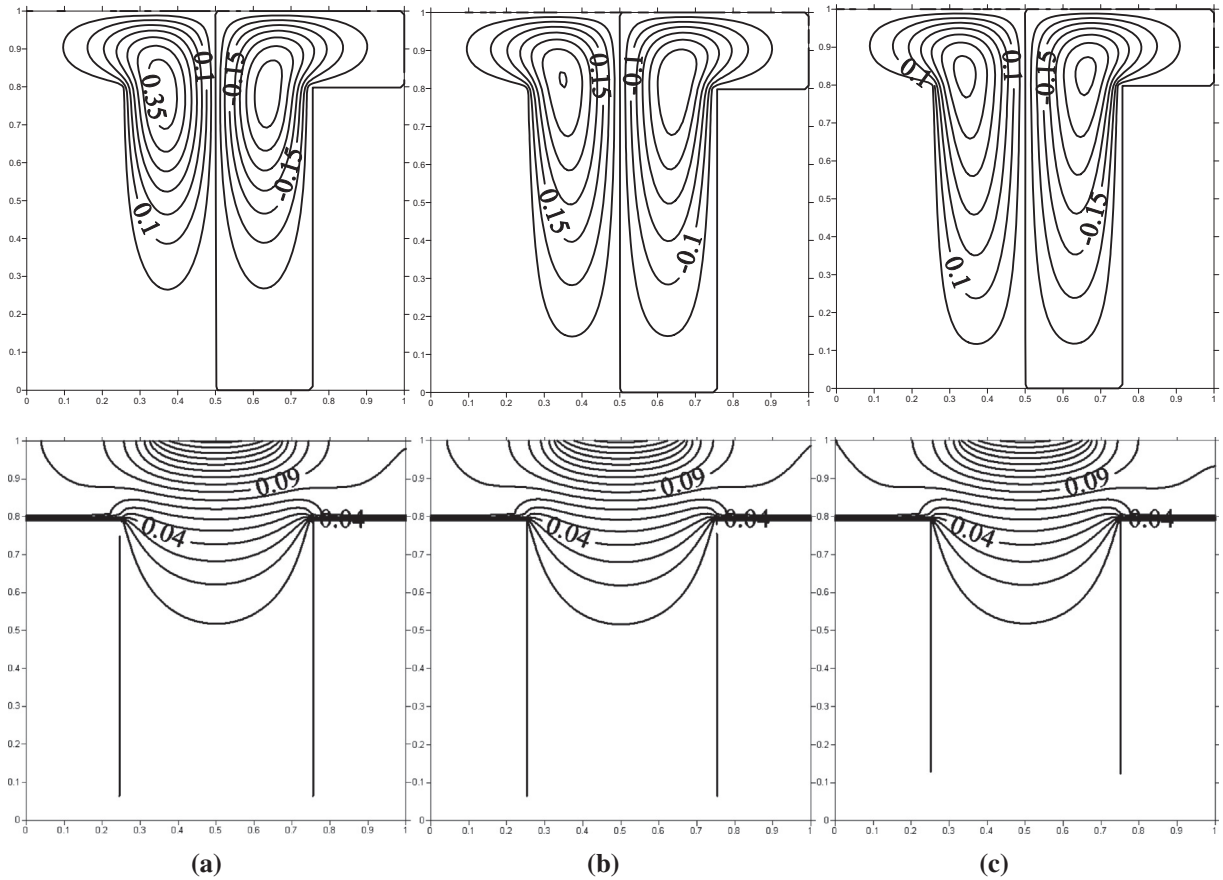

Figure 4 Streamlines (top) and isotherms (down) inside the T-shape enclosure filled with nanofluid ($\phi = 0.1$) at AR = 0.5, $Ra = 10^5$, $B = 0.3$, $D = 0.5$ and $\Phi = 0$ for various Hartmann number [(a) $Ha = 0$, (b) $Ha = 50$, (c) $Ha = 100$].

increase in the fluid viscosity and as a result decreases the flow velocity. Also, it can be noticed that the maximum flow circulation occurs for nanofluid [$\phi = 0.1$], while the minimum flow circulation occurs for pure fluid [$\phi = 0$] for the same reasons explained above. With respect to isotherms, the addition of solid nanoparticles to the base fluid (i.e., water) causes a clear change in their behavior. The results show that the isotherms are converted from irregular shape for pure fluid [$\phi = 0$] and nanofluid with [$\phi = 0.1$] where the convection is dominant to just symmetrical parallel lines for nanofluid with solid volume fraction [$\phi = 0.2$] where the pure conduction is dominant. Since, at high solid volume fraction, less heat is transferred into the enclosure and thus the convection effect decreases.

5.5. Effect of the heat source length and location

Fig. 6 explains streamlines (top) and isotherms (down) inside the T-shape enclosure filled with nanofluid ($\phi = 0.1$) at $Ha = 50$, $Ra = 10^5$, AR = 0.5, $D = 0.5$ and $\Phi = 0$ for various heat source length. It can be observed that the flow circulation decreases as the heat source length increases. This result indicates that, the natural convection enhances when the heat source length decreases. Also, the distribution of the isotherms depends strongly on the heat source length. Note that, the heat source on the top wall transfers most heat into the cold sidewalls of the enclosure leg due to the large temperature difference as can be seen from accumulated isotherms close to the cold sidewalls. With respect to the effect of the heat source location on the streamlines (top) and isotherms (down), the results of Fig. 7 illustrate that the intensity of circulation decreases as the heat source location increases. Also, the isotherms indicated that as the heat source location increases, the heat transfer mode switches from the convection to the conduction.

5.6. Effect of the inclination angle

Fig. 8 explains streamlines (top) and isotherms (down) inside the T-shape enclosure filled with nanofluid ($\phi = 0.1$) at $Ha = 50$, $Ra = 10^5$, AR = 0.5, $B = 0.3$ and $D = 0.5$ for various inclination angle. It can be seen from this figure that as the inclination angle increases, the vortices begin to move upward and compressed in the upper portion of the enclosure. Also, it can be seen from the flow field that as the inclination angle increases from [$\Phi = 0$] to [$\Phi = 90°$], the vortices begin to change their pattern from symmetrical shape to unsymmetrical one. When the inclination angle reaches to 90°, the vortices begin to separate into two major and minor vortices and rotate with a slow rate. On the other hand, no significant effect of inclination angle increasing can be seen on the isotherms contour. The only exception is

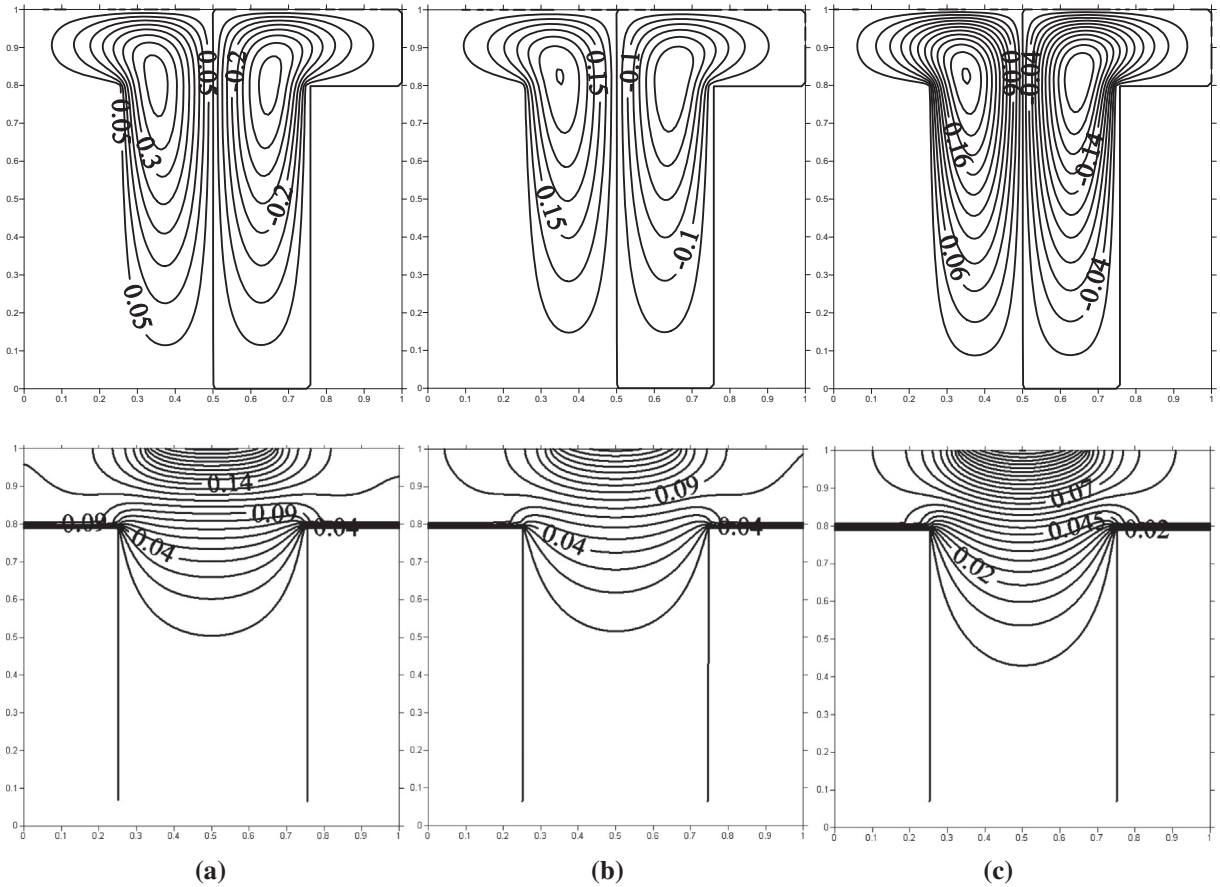

Figure 5 Streamlines (top) and isotherms (down) inside the T-shape enclosure filled with pure and nanofluids at AR = 0.5, $Ra = 10^5$, $B = 0.3$, $D = 0.5$, $Ha = 50$ and $\Phi = 0$ for various solid volume fraction [(a) $\phi = 0$, (b) $\phi = 0.1$, (c) $\phi = 0.2$].

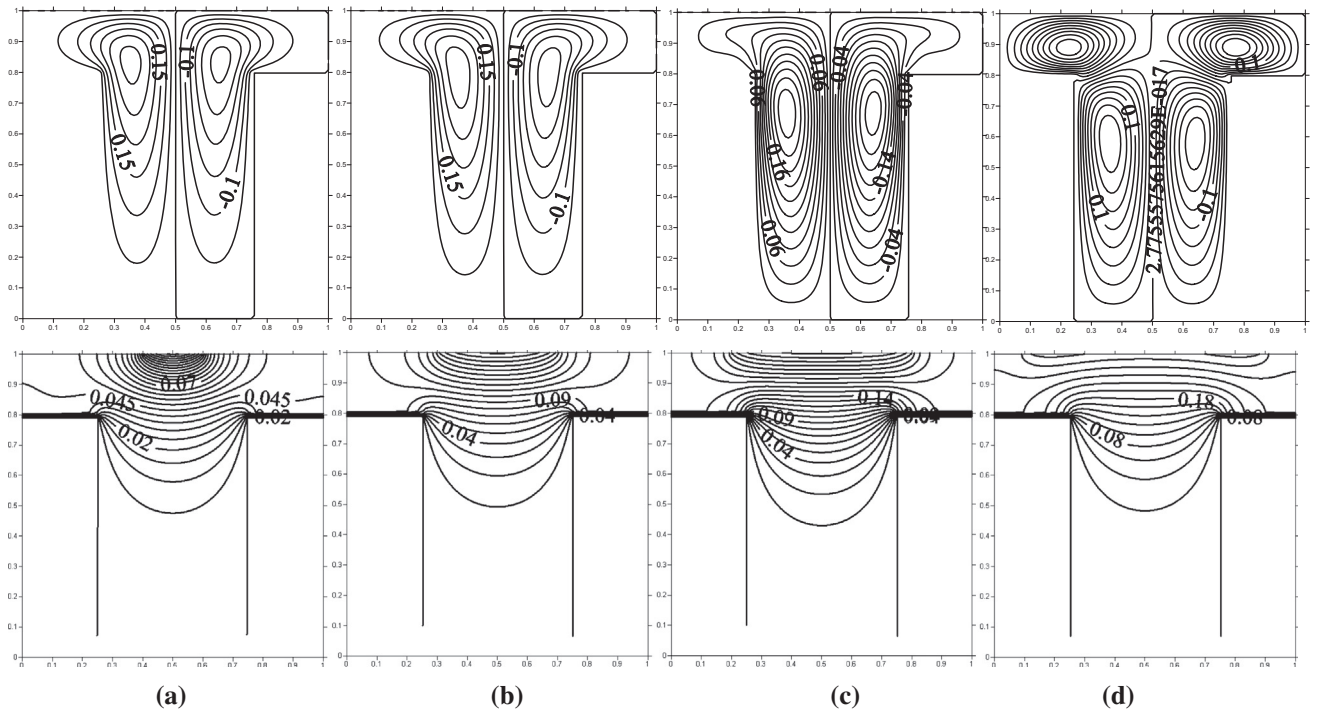

Figure 6 Streamlines (top) and isotherms (down) inside the T-shape enclosure filled with nanofluid ($\phi = 0.1$) at $Ha = 50$, $Ra = 10^5$, AR = 0.5, $D = 0.5$ and $\Phi = 0$ for various heat source length [(a) $B = 0.2$, (b) $B = 0.4$, (c) $B = 0.6$, (d) $B = 0.8$].

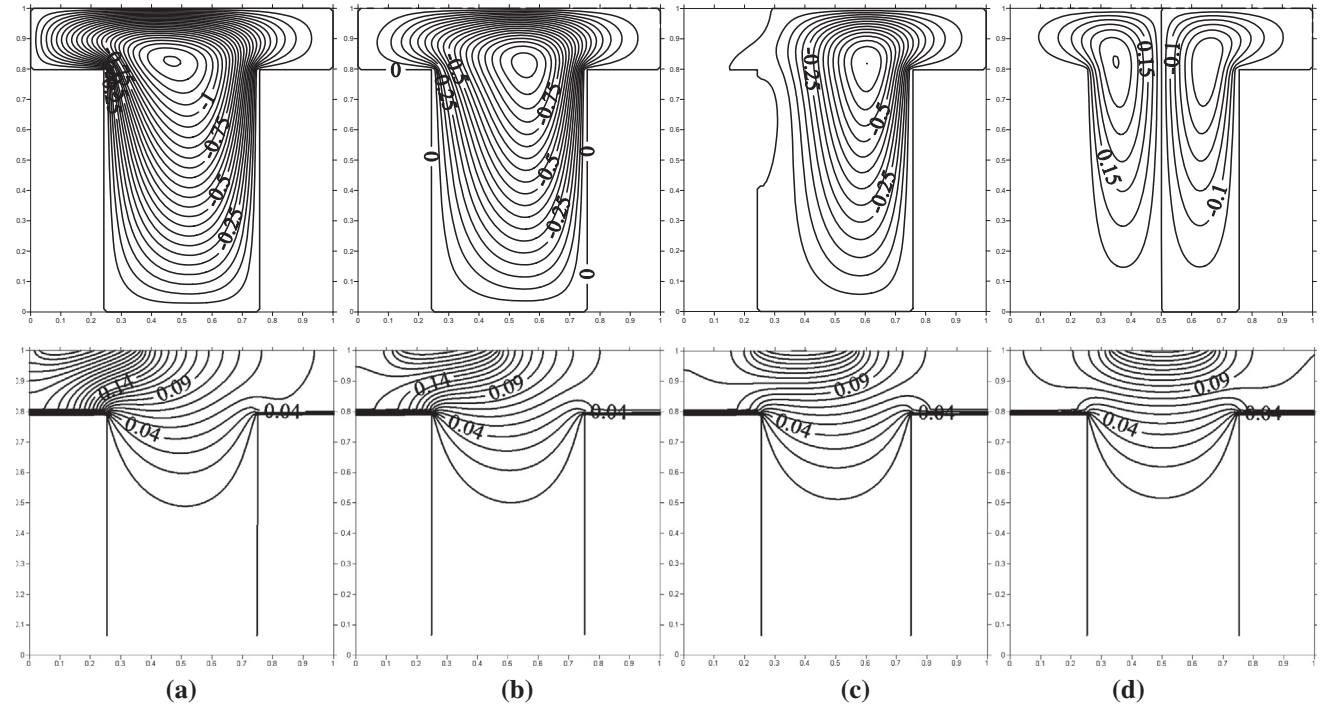

Figure 7 Streamlines (top) and isotherms (down) inside the T-shape enclosure filled with nanofluid ($\phi = 0.1$) at $Ha = 50$, $Ra = 10^5$, AR = 0.5, $B = 0.3$ and $\Phi = 0$ for various heat source location [(a) $D = 0.2$, (b) $D = 0.3$, (c) $D = 0.4$, (d) $D = 0.5$].

when $\Phi = 90°$, where isotherm lines are extended clearly inside the enclosure and diverge far away from the heat source. This is due to the dominance of heat conduction at [$\Phi = 90°$].

5.7. Mean Nusselt number results

Fig. 9 illustrates the variation of mean Nusselt number with solid volume fraction for various Rayleigh number. It can be

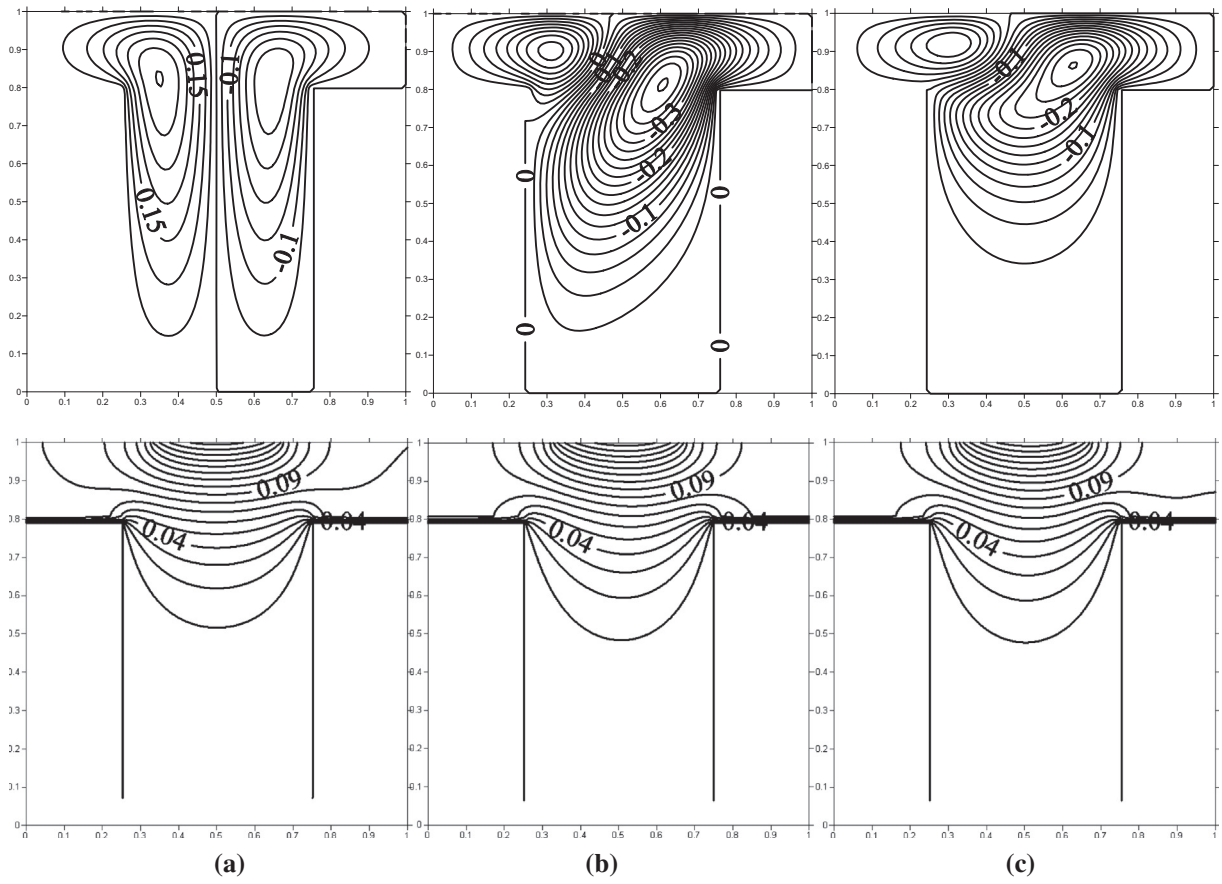

Figure 8 Streamlines (top) and isotherms (down) inside the T-shape enclosure filled with nanofluid ($\phi = 0.1$) at $Ha = 50$, $Ra = 10^5$, AR = 0.5, $B = 0.3$ and $D = 0.5$ for various inclination angle [(a) $\Phi = 0$, (b) $\Phi = 45°$, (c) $\Phi = 90°$].

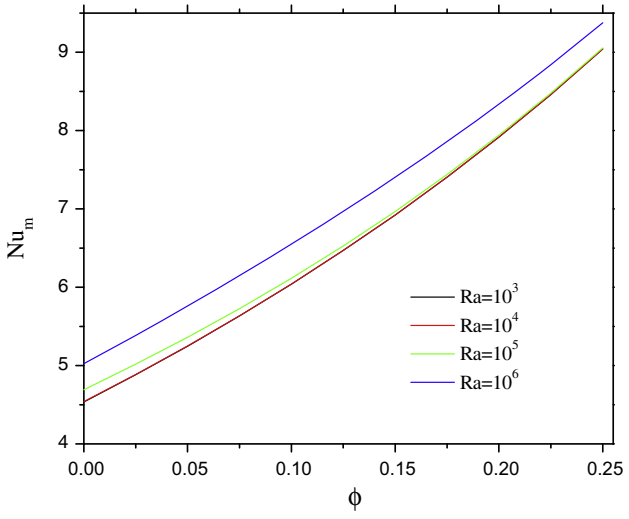

Figure 9 Variation of mean Nusselt number with solid volume fraction for various Rayleigh number.

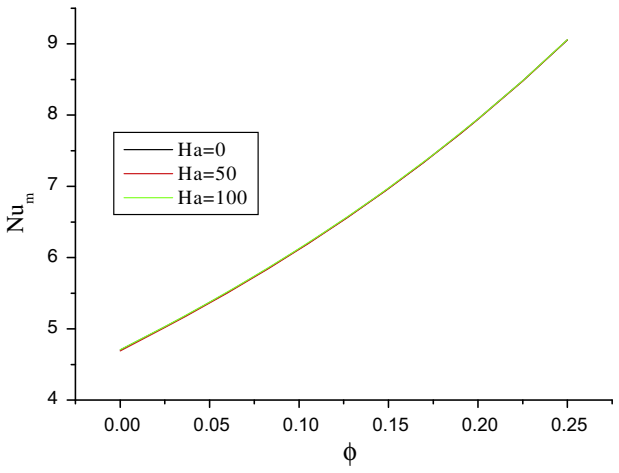

Figure 10 Variation of mean Nusselt number with solid volume fraction for various Hartmann number.

noticed that the average Nusselt number increases with the increase of Rayleigh number and volume fraction of nanoparticles. This is due to the enhancement in the natural convection when the Rayleigh number increases. Moreover, the increase of the solid volume fraction improves the heat transfer in the enclosure and consequently average Nusselt number increases. Fig. 10 shows the variation of mean Nusselt number with solid volume fraction for various Hartmann number. For no magnetic field [i.e., $Ha = 0$], a linear variation can be seen between the mean Nusselt and solid volume fraction. But as

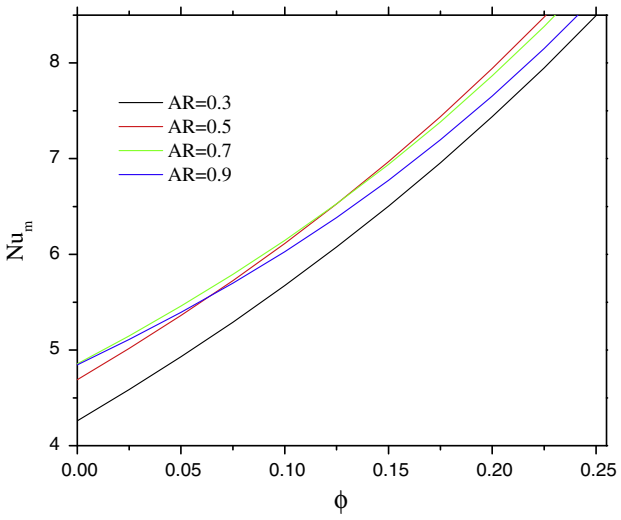

Figure 11 Variation of mean Nusselt number with solid volume fraction for various aspect ratio.

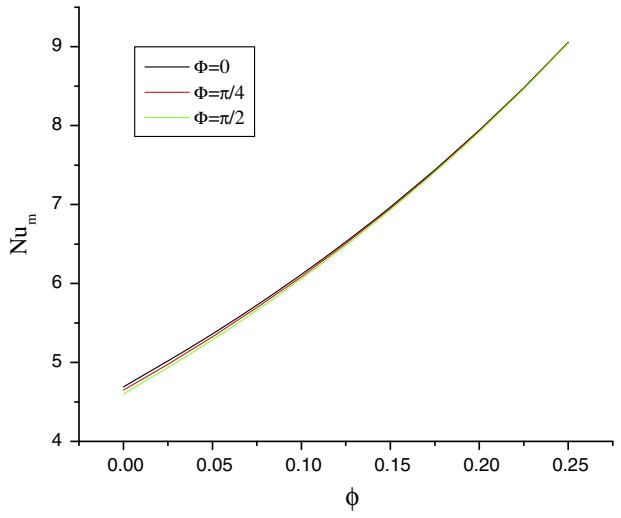

Figure 12 Variation of mean Nusselt number with solid volume fraction for various inclination angle.

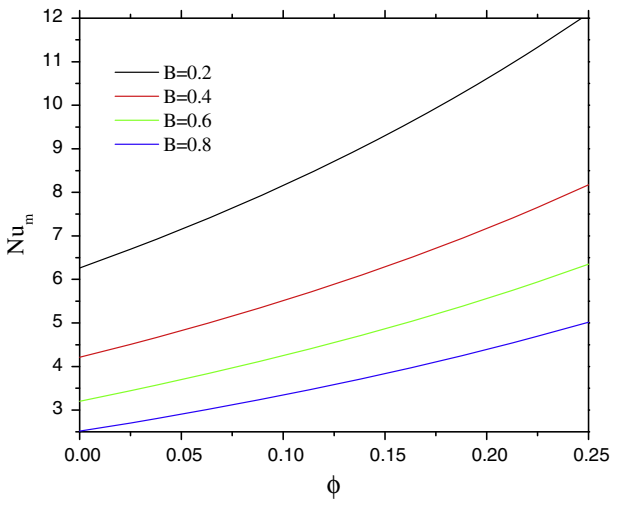

Figure 13 Variation of mean Nusselt number with solid volume fraction for various heat source length.

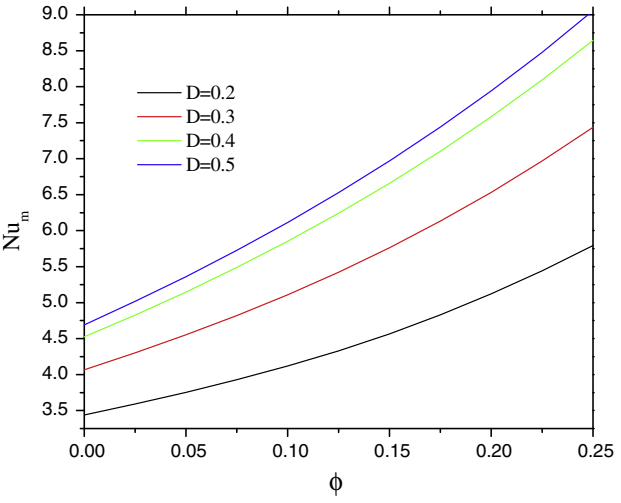

Figure 14 Variation of mean Nusselt number with solid volume fraction for various heat source location.

the Hartmann number begins to increase, the mean Nusselt number decreases gradually. This is because, the effect of magnetic field becomes significant when the Hartmann number increases. In this case, the magnetic force effect becomes greater than the buoyancy force effect and leads to reduce the mean Nusselt number values. Therefore, the magnetic force is the dominant force and controls the flow inside the T-shape enclosure causing to reduce the mean Nusselt number. Fig. 11 shows the variation of mean Nusselt number with solid volume fraction for various aspect ratio. The results show that the mean Nusselt number increases as the aspect ratio and solid volume fraction increase. Fig. 12 shows the variation of mean Nusselt number with solid volume fraction for various inclination angle. The results explain that the mean Nusselt number increases with the solid volume fraction for various values of the inclination angle. Fig. 13 illustrates the variation of mean Nusselt number with solid volume fraction for various heat source length. The results show that the mean Nusselt number increases with the solid volume fraction as the heat source length decreases. This is because the natural convection enhances when the heat source length decreases. Fig. 14 shows the variation of mean Nusselt number with solid volume fraction for various heat source location. The results show that the mean Nusselt number increases with the solid volume fraction as the heat source location increases.

6. Conclusions

The following conclusions can be drawn from the results of the present work:

1. When the aspect ratio of the enclosure increases, a clear improvement in the flow circulation occurs.
2. When the aspect ratio of the enclosure increases, the heat transfer mode switches from the conduction to the convection.

3. The natural convection enhances when the heat source length and its location decrease.
4. When the Rayleigh number increases and the Hartmann number decreases, the enhancement in the flow circulation leads to make the isotherms irregular and curved in shape and the heat convection dominates. A reverse behavior can be seen when the Rayleigh number decreases and the Hartmann number increases.
5. When the solid volume fraction increases from [$\phi = 0$] to [$\phi = 0.1$], the circulation intensity increases as a result of the high energy transport through the flow related with the high motion of nanoparticles. But as the solid volume fraction increases further to $\phi = 0.2$, the stream function values begin to decrease strongly.
6. The mean Nusselt number increases with the increase of Rayleigh number, aspect ratio and, inclination angle and volume fraction of nanoparticles.
7. When the Hartmann number increases, the mean Nusselt number decreases.
8. No significant effect is noticed in the isotherms when the enclosure inclination angle increases. While, the vortices begin to change their pattern from symmetrical shape to unsymmetrical one as the inclination angle increases from [$\Phi = 0$] to [$\Phi = 90°$].
9. The mean Nusselt number increases with the solid volume fraction for various values of the inclination angle.
10. The mean Nusselt number increases with the solid volume fraction as the heat source length decreases and its location increases.

References

[1] L. Kolsi, A. Hussein, M. Borjini, H. Mohammed, H. Ben Aïssia, Computational analysis of three-dimensional unsteady natural convection and entropy generation in a cubical enclosure filled with water-Al_2O_3 nanofluid, Arab. J. Sci. Eng. 39 (2014) 7483–7493.

[2] S. Ahmed, A. Hussein, H. Mohammed, S. Sivasankaran, Boundary layer flow and heat transfer due to permeable stretching tube in the presence of heat source/sink utilizing nanofluids, Appl. Math. Comput. 238 (2014) 149–162.

[3] A. Hussein, H. Ashorynejad, M. Shikholeslami, S. Sivasankaran, Lattice Boltzmann simulation of natural convection heat transfer in an open enclosure filled with Cu–water nanofluid in a presence of magnetic field, Nucl. Eng. Des. 268 (2014) 10–17.

[4] M. Mahmoodi, Numerical simulation of free convection of a nanofluid in L-shaped cavities, Int. J. Therm. Sci. 50 (2011) 1731–1740.

[5] M. Mahmoodi, S. Hashemi, Numerical study of natural convection of a nanofluid in C-shaped enclosures, Int. J. Therm. Sci. 55 (2012) 76–89.

[6] R. Dehnavi, A. Rezvani, Numerical investigation of natural convection heat transfer of nanofluids in a Γ shaped cavity, Superlattices Microstruct. 52 (2012) 312–325.

[7] M. Mansour, A. Bakier, M. Bakier, Natural convection of the localized heat sources of T-shaped nanofluid-filled enclosures, Am. J. Eng. Res. 2 (7) (2013) 49–61.

[8] M. Ali, O. Zeitoun, S. Almotairi, Natural convection heat transfer inside vertical circular enclosure filled with water-based Al_2O_3 nanofluids, Int. J. Therm. Sci. 63 (2013) 115–124.

[9] M. Kalteh, H. Hasani, Lattice Boltzmann simulation of nanofluid free convection heat transfer in an L-shaped enclosure, Superlattices Microstruct. 66 (2014) 112–128.

[10] M. Rahman, S. Saha, S. Mojumder, S. Mekhilef, R. Saidur, Numerical simulation of unsteady heat transfer in a half-moon shape enclosure with variable thermal boundary condition for different nanofluids, Numer. Heat Transf., Part B 65 (2014) 282–301.

[11] S. Mahmud, Free convection inside an L-shaped enclosure, Int. Commun. Heat Mass Transf. 29 (2002) 1005–1013.

[12] A. Hussain, S. Hussain, Heatline visualization of natural convection heat transfer in an inclined wavy cavities filled with nanofluids and subjected to a discrete isoflux heating from its left sidewall, Alex. Eng. J. 55 (2016) 169–186.

[13] S. Soleimani, M. Sheikholeslami, D. Ganji, M. Gorji-Bandpy, Natural convection heat transfer in a nanofluid filled semi-annulus enclosure, Int. Commun. Heat Mass Transf. 39 (2012) 565–574.

[14] M. Sheikholeslami, M. Gorji-Bandpy, S. Seyyedi, D. Ganji, H. Rokni, S. Soleimani, Application of LBM in simulation of natural convection in a nanofluid filled square cavity with curve boundaries, Powder Technol. 247 (2013) 87–94.

[15] M. Ali, O. Zeitoun, S. Almotairi, H. Al-Ansary, The effect of alumina-water nanofluid on natural convection heat transfer inside vertical circular enclosures heated from above, Heat Transf. Eng. 34 (15) (2013) 1289–1299.

[16] M. Al-Hafidh, H. Mohammed, Natural convection of nanofluid in cylindrical enclosure filled with porous media, J. Energy Power Eng. 7 (2013) 2263–2272.

[17] M. Uddin, M. Kabir, O. Anwar Beg, Computational investigation of Stefan blowing and multiple slips effect on buoyancy-driven bioconvection nanofluid flow with microorganisms, Int. J. Heat Mass Transf. 95 (2016) 116–130.

[18] M. Uddin, O. Anwar Beg, M. Uddin, Multiple slips and variable transport property effect on magnetohydromagnetic dissipative thermosolutal convection in a porous medium, J. Aerospace Eng. (2016), http://dx.doi.org/10.1061/(ASCE)AS.1943-5525.0000614.

[19] M. Uddin, M. Kabir, Y. Alginahi, Lie group analysis and numerical solution of magnetohydrodynamic free convective slip flow of micropolar fluid over a moving plate with heat transfer, Comput. Math. Appl. 70 (5) (2015) 846–856.

[20] N. Abdul Latiff, M. Uddin, O. Anwar Beg, A. Ismail, Unsteady forced bioconvection slip flow of a micropolar nanofluid from a stretching/shrinking sheet, Proc. Inst. Mech. Eng. Part N: J. Nanomater. Nanoeng. Nanosyst. (2015), http://dx.doi.org/10.1177/1740349915613817.

[21] M. Uddin, B. Rostami, M. Rashid, P. Rostami, Similarity and analytical solutions of free convective flow of Dilatant nanofluid in a Darcian porous medium with multiple convective boundary conditions, Alex. Eng. J. 55 (2016) 263–274.

[22] E. Sourtiji, S. Hosseinizadeh, Heat transfer augmentation of magneto-hydrodynamics natural convection in L-shaped cavities utilizing nanofluids, Therm. Sci. 16 (2) (2012) 489–501.

[23] M. Sheikholeslami, M. Gorji-Bandpy, D. Ganji, S. Soleimani, Effect of a magnetic field on natural convection in an inclined half-annulus enclosure filled with Cu-water nanofluid using CVFEM, Adv. Powder Technol. 24 (2013) 980–991.

[24] M. Sheikholeslami, M. Gorji-Bandpy, D. Ganji, Numerical investigation of MHD effects on Al_2O_3-water nanofluid flow and heat transfer in a semi-annulus enclosure using LBM, Energy 60 (2013) 501–510.

[25] A. Al-Zamily, Effect of magnetic field on natural convection in a nanofluid-filled semi-circular enclosure with heat flux source, Comput. Fluids 103 (2014) 71–85.

[26] M. Sheikholeslami, D. Ganji, M. Gorji-Bandpy, S. Soleimani, Magnetic field effect on nanofluid flow and heat transfer using KKL model, J. Taiwan Inst. Chem. Eng. 45 (2014) 795–807.

[27] M. Sheikholeslami, M. Gorji-Bandpy, D. Ganji, P. Rana, S. Soleimani, Magnetohydrodynamic free convection of Al_2O_3–water nanofluid considering thermophoresis and Brownian motion effects, Comput. Fluids 94 (2014) 147–160.

[28] S. Hussain, A. Hussein, Natural convection heat transfer enhancement in a differentially heated parallelogrammic enclosure filled with copper-water nanofluid, J. Heat Transf. – Trans. ASME 136 (2014) 1–8.
[29] M. Mansour, R. Mohamed, M. Abd-Elaziz, S. Ahmed, Numerical simulation of mixed convection flows in a square lid-driven cavity partially heated from below using nanofluid, Int. Commun. Heat Mass Transf. 37 (2010) 1504–1512.
[30] M. Mansour, A. Chamkha, R. Mohamed, M. Abd El-Aziz, S. Ahmed, MHD natural convection in an inclined cavity filled with a fluid saturated porous medium with heat source in the solid phase, Nonlinear Anal.: Modell. Control 15 (1) (2010) 55–70.
[31] T. Grosan, C. Revnic, I. Pop, D. Ingham, Magnetic field and internal heat generation effects on the free convection in a rectangular cavity filled with a porous medium, Int. J. Heat Mass Transf. 52 (2009) 1525–1533.
[32] B. Ratish Kumar, P. Murthy, P. Singh, Free convection heat transfer from an isothermal wavy surface in a porous enclosure, Int. J. Numer. Meth. Fluids 28 (1998) 633–661.